PHOTONICS Research

Adaptive cavity-enhanced dual-comb spectroscopy

Weipeng Zhang,[1] Xinyi Chen,[1] Xuejian Wu,[2] Yan Li,[1] and Haoyun Wei[1,*]

[1]State Key Laboratory of Precision Measurement Technology & Instruments, Department of Precision Instrument, Tsinghua University, Beijing 100084, China
[2]Department of Physics, 366 Le Conte Hall MS 7300, University of California, Berkeley, California 94720, USA
*Corresponding author: luckiwei@mail.tsinghua.edu.cn

Received 2 April 2019; revised 21 May 2019; accepted 19 June 2019; posted 21 June 2019 (Doc. ID 363972); published 23 July 2019

Resolution and bandwidth are critical for cavity-enhanced dual-comb spectroscopy (CE-DCS). Here, we pioneer an adaptive approach in CE-DCS to improve the broadband as well as the resolution. Postcorrections to dual-comb interferograms adaptively compensate the relative phase jitters of the optical frequency combs and result in both a mode-resolved spectral resolution and a signal-to-noise ratio of 440:1 in 1 s. Meanwhile, an adaptive comb-cavity locking scheme exploits more than 90% of the comb modes, covering 340 cm^{-1} (10 THz) at 6450 cm^{-1}. For a single dual-comb interferogram, more than 40,000 comb teeth spaced by 250 MHz are measured in less than 7.5 ms, contributing to a noise equivalent absorption per spectral element of 2×10^{-10} $cm^{-1} \cdot Hz^{-1/2}$. This adaptive cavity-enhanced dual-comb spectroscopy technique provides an attractive spectroscopic tool that may be utilized in trace-gas sensing, breath and cancer analysis, and engine combustion diagnosis.

https://doi.org/10.1364/PRJ.7.000883

1. INTRODUCTION

Cavity-enhanced optical frequency comb spectroscopy (CE-OFCS) marries broadband spectrum with high sensitivity, and thus permits spectroscopy in cold molecules probing [1], chemical kinetics analysis [2], flame diagnosis [3], breath analysis [4], and remote sensing [5,6]. It requires not only the perfect coupling of the comb into a cavity but also an effective technique for resolving and detecting the comb elements. Even though their analogous equidistant modes provide the very intuition of their integrations, matching the two degrees of freedom (DOFs) of the comb, namely, the repetition rate (f_{rep}) and the carrier envelope offset (f_{ceo}), with the only parameter of the cavity, the free spectral range (FSR), can be challenging. A two-point locking scheme [7,8] intuitively fits the two DOFs of the comb to the cavity but has defects in increasing complexity and in limiting the coupled optical power and bandwidth, since, in some implementations [9], modulation is applied directly to the comb light. The one-point locking scheme [10–12], which inversely locks the cavity to the comb, circumvents these problems. But previous practices have imperfections in nonconstant transmitting [12], showing incompetent stability for the dual-comb technique. Steady coupling is realized in a recent work [10], yet a short length cavity is used for portability, suffering from a large mode-spacing of 2 GHz and multiple steps of sweeping of cavity length for coupling every adjacent comb tooth. For measuring the transmitted comb light, various configurations are attempted, such as the cavity ring-down [13], employing dispersers [14–16], the Vernier methods [17–19], the mechanical Fourier transform spectrometers (FTSs) [9,20], and dual-comb spectroscopy (DCS) [10,21,22]. Among these, the DCS potentially stands out in subgigahertz resolution and submicrosecond detecting speed [23–27]. The debut of the CE-DCS [22], however, fails to be superior in spectral resolution, which is 4.5 GHz and is still surpassed by the mechanical FTS ones. This is, to a large extent, due to the deteriorated mutual coherence caused by the phase fluctuations between the two combs [28], only permitting a resolution 10 times worse than the ideal value. Locking the combs to two optical frequencies can be effective solutions [10,27], but there is a sacrifice in cost and complexity. Another implementation uses the combs generated by electro-optical modulating of the continuous-wave (CW) lasers, revealing less complexity and even higher mutual coherence [21]. But these combs emit a narrow spectrum spanning no wider than 0.41 cm^{-1} (50 GHz), which is insufficient for the simultaneous analysis of multiple spectral bands and molecules. The dawn of the adaptive methods [29–33], which compensate the distorted interferograms (IGMs), enables simple configurations as well as high resolution. Up till now, no such an adaptive approach with the cavity-enhanced setup has happened.

In this paper, we demonstrate an adaptive cavity-enhanced dual-comb spectroscopy (ACE-DCS) that realizes high spectral resolution, high sensitivity, and broad spectral bandwidth. The adaptive postcorrections of the IGMs are implemented, achieving a signal-to-noise ratio (SNR) of 440:1 in 1 s and a mode-resolved resolution (250 MHz), and eliminating the

tight-locking of the comb to state-of-the-art lasers. Meanwhile, an adaptive comb-cavity coupling scheme, including the optimizations of the two comb parameters and the Pound–Drever-Hall (PDH) technique, tightly locks the cavity length to adaptively track the variation of the comb. These bring about better coupling stability, a broader spectrum (>10 THz), and, to the best of our knowledge, the largest number (>40,000) of spectral elements among the CE-OFCS techniques. This ACE-DCS technique potentially facilitates precision spectroscopy, including atmospheric trace-gas observation, rapid breath analysis, and dynamic combustion diagnosis.

2. PRINCIPLE

In our ACE-DCS setup, we demonstrate an adaptive comb-cavity coupling. Apart from tuning the f_{rep} and f_{ceo} of the comb for optimizing the coupling bandwidth, a CW laser is added as an intermediary that adaptively locks the cavity length and permits robust and constant comb-to-cavity coupling.

The first step in this one-point coupling approach is to optimize the repetition rate of the comb. Notably, when sweeping the cavity length, for the two cases that the f_{rep} is greater [Fig. 1(a)] or lower [Fig. 1(b)] than the FSR, this envelope moves in opposite directions and transmits different portions of the comb spectrum. Such a characteristic provides a criterion for adjusting the FSR. When sweeping the cavity, if the current f_{rep} locates within the dithering range of the FSR, two adjacent transmitted peaks of the comb that have horizontally symmetrical shapes should be found, as shown in Fig. 1(d). Otherwise, as shown in Fig. 1(c), the f_{rep} needs further adjustment. Next, tuning the value of f_{ceo} until observing three adjacent transmission peaks and the two symmetrical ones that lie on the sides have equal intensities, as shown in Fig. 1(e), optimizes the transmission power of the center peak.

Then, the cavity length should be locked to permit the highest transmitted power of the comb, the $L_{matched}$ in Fig. 1(e). Previous one-point coupling adopts the dither-locking method, which, unfortunately, is incapable of a tight-locking performance due to its large response latency. Also, unwanted phase shift to the coupled comb light is introduced because the locking point

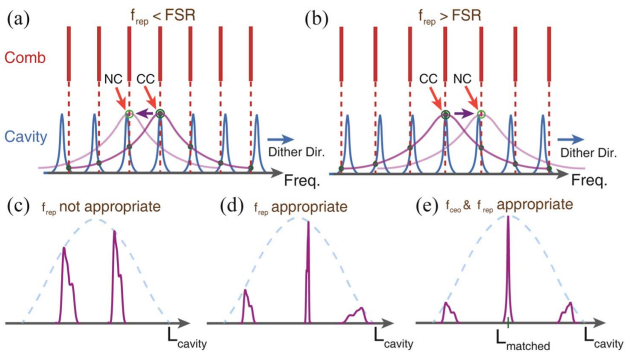

Fig. 1. Adjustment of f_{rep} and f_{ceo}. Cavity filtering on comb when (a) f_{rep} < FSR and when (b) f_{rep} > FSR. CC, current filtering center; NC, next filtering center. Cavity transmission when (c) f_{rep} is not appropriate, (d) f_{rep} is appropriate and (e) both f_{rep} and f_{ceo} are appropriate.

locates at the side of the transmission peak rather than at the highest point. To overcome these, we innovate the approach by using a CW laser to lock the cavity length adaptively through a sideband PDH technique. The principle is that, on the one hand, the output of the CW laser is phase-modulated by an electro-optical modulator (EOM). Then the PDH technique generates error signals using the carrier frequency and one sideband, which are reflected by the mirror, and locks the rest of the sidebands into the cavity. On the other hand, the light of the CW laser without the modulation is coupled with the comb, their beat note is detected, and frequency is discriminated and used for feedback controlling the cavity length, locking the beat note at the modulating frequency of the EOM. Analogous to the frequency-agile rapid scanning spectroscopy (FARS) [34], the locked comb tooth shares the same frequency with the locked sideband, and thus, the comb is coupled into the cavity with a spectral center close to the frequency of the CW laser. As a supplement to the optimization of the comb parameters in the previous steps, tuning the frequency of the CW laser to the spectral center of the comb can further widen the coupled bandwidth. Because the "equal intensities" used in previous implementations may be relatively imprecise, additional fine-tuning of the f_{ceo} could further optimize the coupled spectrum. Once such adjustments are made, the steady coupling status can be maintained because the cavity length is constantly traced to the same comb tooth. That is to say, the length of the cavity is tuned accordingly to follow the jitters of the f_{ceo} and the f_{rep}.

For obtaining a mode-resolved resolution, a postcorrecting method is adopted. In DCS, the jittering between each pair of comb teeth can be equivalent to the difference of the repetition rate, meaning insufficient stability for resolving each comb element. Our approach can remedy this through retrieving the phase jittering of the two combs using two CW lasers and applying adaptive corrections to the IGMs [32,33]. In our setup, the CW laser used for the comb-cavity coupling can also work for this adaptive correction, and only one additional CW laser with a different operating wavelength is needed. These two CW lasers beat with the two combs, and the four generated beat notes are used for the postcorrection algorithm. The details of this algorithm are described in the Appendix A. Through the mixing and resampling of the original IGMs, the corrected IGMs are free from the effects of both the f_{rep} jitters and the f_{ceo} jitters.

Thanks to the stable transmission maintained by the adaptive comb-cavity coupling and the error-free IGMs produced by the postcorrections, high-quality dual-comb measurements can be continuously obtained. Subsequently, applying the direct time domain averaging using multiple IGMs, higher SNRs can result.

3. EXPERIMENTAL SETUP

The experimental setup, shown in Fig. 2, consists of a measurement part and an acquisition part. In Fig. 2(a), the output of an external cavity diode laser (ECDL) (Newport, TLB-6728) was divided into three equal power portions. The first portion was phase-modulated by an EOM (Newport, 4002) that generated sidebands for the PDH locking at a detuning frequency of 20 MHz. A phase shifter adjusted the polarity of the PDH error

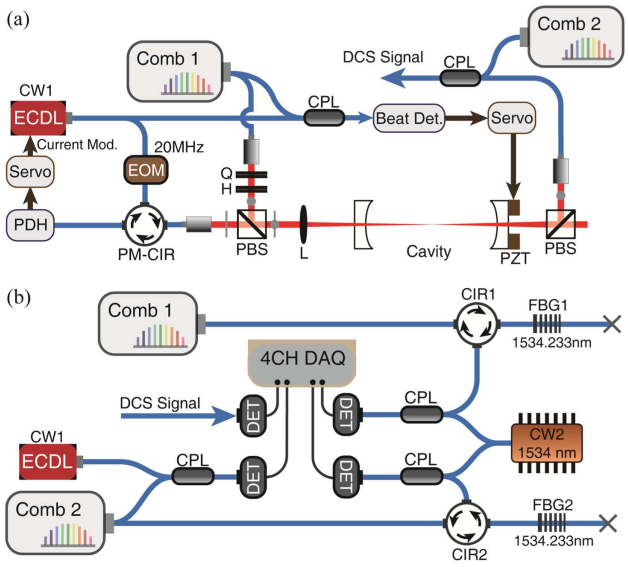

Fig. 2. Experimental setup. (a) Measurement part; (b) acquisition part. ECDL, external cavity diode laser; CW1, CW2, continuous-wave lasers; PDH, Pound–Drever-Hall detection; EOM, electro-optical modulator; CPL, coupler; PBS, polarization beam splitter; L, lens; PZT, piezo actuator; DCS, dual-comb spectroscopy; Q, quarter-wave plate; H, half-wave plate; blue lines, optical fibers; red lines, spatial beams.

signal to move the locking point of the proportion-integration (PI) controller (Newport, LB1005) to one of the sidebands. Another output portion of the ECDL beat with Comb1 (Menlosystems, FC-250-1500). When the ECDL was locked to the cavity, the frequency of the ECDL followed with the cavity length, which in turn varied its beating frequency with the comb. Using a phase discriminator (Menlosystems, DXD 200) and a PI controller, we feedback-controlled the piezo actuator (PZT) mounted on the cavity mirror and locked the beating to the same frequency of the EOM (20 MHz). All the RF signals, including the modulating source of the EOM and the sampling clock of the data acquisition device, were synchronized to the same rubidium clock (Symmetricom, 8040C), which was also the reference of the combs. Thus, the beating comb tooth shared the same frequency with the ECDL sideband and could be coupled into the cavity. The last portion of the ECDL output was used for the acquisition part and will be explained later. The enhancement cavity, as shown in Fig. 2(a), is approximately 600 mm long, corresponding to an FSR of about 250 MHz, close to the repetition rate of the combs. The reflectivity of the cavity mirror is higher than 99.95% within the whole spectral range of the comb, denoting a finesse of around 3000. Four invar rods supported the cavity for stabilizing the cavity length, and a sandwich of heater and insulation cotton maintained the temperature with a thermostat (Wavelength Electronics, PTC-2.5 K). There are three inlets and outlets along the cavity, which were used for exchanging the gas and monitoring the inside pressure.

The acquisition part is shown in Fig. 2(b), wherein one of the two CW lasers that generated the reference signals is the rest portion of the ECDL, as noted above. The other CW laser [CW2, shown in Fig. 2(b)] is a narrow linewidth laser (Redfern Integrated Optics, 1534.233 nm). Because of the low output power of the comb around the wavelength of the CW2, we used two fiber Bragg gratings (FBGs) to improve the SNR of the beat notes. The comb power around the ECDL frequency was sufficient for omitting the use of FBGs. Since the beat note between Comb1 and the ECDL was tightly locked to 20 MHz with subhertz jittering (in the measurement part), this beat signal can be numerically constructed, and is needless for being recorded. Compared to Ref. [33], the required acquisition channels are reduced by one, and only a four-channel acquisition board (NI 5761, 14 bits, 250 MS/s) was used for synchronously digitizing the three beat notes and the dual-comb IGMs. Although in Ref. [32], two balanced detectors are used for simultaneously recording four beat notes using just two acquisition channels, only three channels are needed. But, in that setup, additional numerical filtering is required, and the effective dynamic range of the each digitizing beat note is reduced. We adopted a bandpass filter (17–32 MHz) for recording the DCS signal, which could help avoid frequency aliasing and increase the SNR. The maximum recording time is 1 s, limited by the size of the onboard memory. Since the acquisition card was populated with a field-programmable gate array (FPGA), it can be used for real-time processing of the IGMs and circumvent the limited acquisition time.

4. RESULTS

According to the adjustment procedure mentioned in Section 2, we recorded the transmitted optical power when sweeping the cavity length, as shown in Figs. 3(a)–3(c);

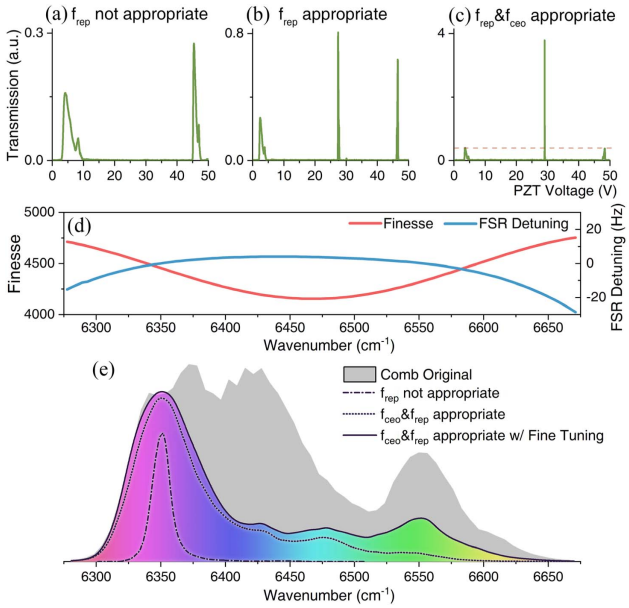

Fig. 3. Optimization of f_{rep} and f_{ceo} and coupled spectrum. Cavity transmission in the experiment when (a) f_{rep} is not appropriate, (b) f_{rep} is appropriate, and (c) f_{rep} and f_{ceo} are appropriate. The nonuniform intervals between adjacent two peaks appearing in (b) and (c) were due to the nonlinearity of the piezo movement. (d) Cavity finesse and corresponding frequency detuning of FSR. (e) The spectra of the original comb and the transmitted light in cases of (a), (c), and fine-tuning of f_{ceo}.

the corresponding spectrum is shown in Fig. 3(e). In case that the f_{rep} was not fully matched with FSR, only a bandwidth of 30 cm^{-1} and an optical power of 0.5 mW could be coupled. After adjusting the two parameters of the comb until we got two peaks of identical height, as shown in Fig. 3(c), we further fine-tuned the f_{ceo} to find the widest coupled bandwidth, shown as the light blue in Fig. 3(e). The determined optimal values of the f_{rep} and f_{ceo} of the Comb1 were 250 and −65 MHz.

Thanks to the fine-tuning of comb parameters and the tight locking of the ECDL, the final optimized optical power was 3.6 mW, which is more than 17% of the incident comb power; the corresponding coupled bandwidth stably exceeded 340 cm^{-1}(6300 – 6640 cm^{-1}). Thus, a spectral bandwidth of over 10 THz is available for DCS measurement. Since the FSR of the cavity is the same as the f_{rep} of the combs, almost every comb tooth was coupled within the entire bandwidth of the comb output, with a total number of more than 40,000. The coupled bandwidth can be potentially further widened if the comb is spectrally expanded using nonlinear fiber optics. These results convincingly attest to the feasibility of this one-point cavity-comb coupling. It is fair to say the coupled comb intensity and the bandwidth were degraded compared to the original comb, the reason for which can be complicated. First, due to the dispersion of the cavity mirror, the modes of the cavity are not strictly equidistant, as indicated by the cavity finesse shown in Fig. 3(d). Thus, even if the comb modes around the frequency of the CW1 laser have perfect alignment with the cavity, modes at frequencies away from the CW1 laser may reveal mismatching with the cavity. Second, the response bandwidth of the PZT that is mounted on the cavity mirror is typically small and may raise instability of the PDH locking, causing the degradation of the coupling efficiency.

To demonstrate this ACE-DCS spectrometer, we measured rovibrational transitions of the N_2O gas sample around 1.5 μm (6300 – 6650 cm^{-1}), which covers four spectral bands, namely, the (4200 → 0000), the (5000 → 0000), the (0113 → 0110), and the (0003 → 0000). The gas sample had a purity of more than 99.9% and was detected at a pressure of around 420 Pa and a temperature of 298 K. According to the passband of the filter and the determined parameters of Comb1, as mentioned above, we set the f_{rep} and f_{ceo} of Comb2 to be 250.00014 and 20 MHz. Thus, according to Ref. [27], the frequency of the IGMs located within 20 to 25 MHz, and the measurement rate was 140 Hz. Figure 4(a) is the spectrum after applying Fourier transform to a measured

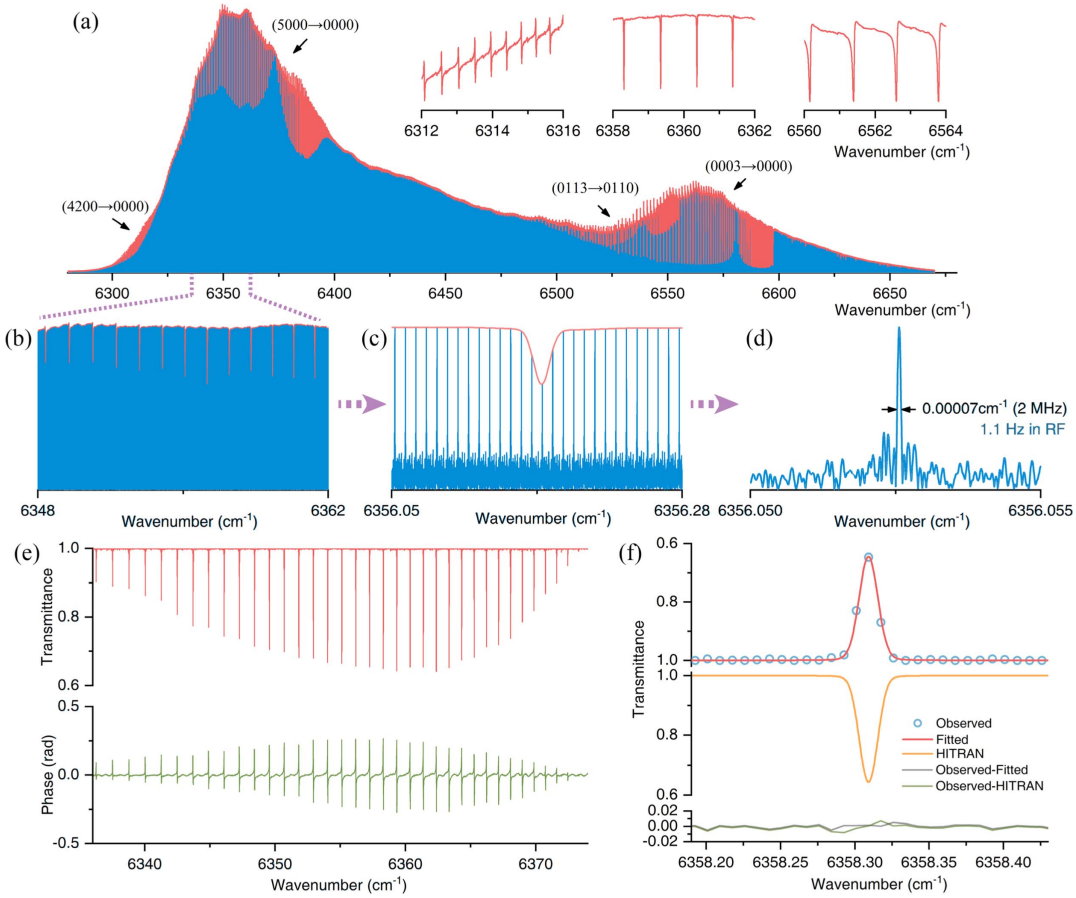

Fig. 4. Spectral measurement of ACE-DCS system. (a) The spectrum of N_2O sample around 6450 cm^{-1}; blue lines, the measured spectrum after Fourier transforming the IGM, exhibiting each individual comb mode; red lines, the fitted spectrum using the highest points of each comb mode, revealing clear absorption features. (b), (c), and (d) Mode-resolved spectrum in different scales, spanning 14 cm^{-1}, 0.23 cm^{-1}, and 0.005 cm^{-1}, respectively. (e) Transmittance and phase around 6370 cm^{-1}; (f) transmittance of the P(16) line of the (5000 → 0000) band and the Voigt fitted result and the line profile provided by HITRAN 2016.

IGM with a recording time of 1 s. As shown in the inset of Fig. 4, the different regions of the spectrum all reveal clear features of absorption transitions. The "overshoot" baselines, shown around 6314 cm^{-1} and 6562 cm^{-1}, are due to the misalignment between the cavity modes and the comb teeth caused by the mirror dispersion, which commonly happens for broadband cavity-enhanced frequency comb spectroscopy and has proved to be compensated when taking the dispersion parameters into the fitting process [10,35]. Figures 4(b)–4(d) and the zoomed-in spectrum, where each comb line can be distinguished, confirm the effectiveness of the adaptive postcorrection algorithm and a mode-resolved resolution of this ACE-DCS system.

After truncating the IGM of 1 s into 140 individual IGMs, we averaged them in the time domain and applied Fourier transform. Then we extracted the baseline and got the transmittance and the phase, both of which reveal good quality, as shown in Fig. 4(e). Figure 4(f) shows the observed transmittance for the P(16) line of the (5000 → 0000) band and its fitted curve using the Voigt line shape model. According to this plot, we calculated the SNR using the standard deviation of the transmittance, where no transition lines appear [10,22]. This calculation of SNR is intensity-normalized, and our system obtained a good SNR of higher than 440:1 (in 1 s). Compared to the theoretical line profile using the parameters provided by the HITRAN database [36], as shown in Fig. 4(f), we estimated the actual absorption length to be about 560 m, and the corresponding enhancement coefficient is higher than 900. Given the number of spectral elements of about 40,000 (span/resolution), the noise equivalent absorption (NEA) per spectral element [37] is determined to be 2.0×10^{-10} $cm^{-1} \cdot Hz^{-1/2}$, showing more than a tenfold improvement over the latest CE-DCS setup [10]. Compared to the cavity ringdown spectroscopy [38], this ACE-DCS system also reveals a commensurate sensitivity and outstands because of its broadband measurement ability.

5. CONCLUSION

In summary, we developed an adaptive cavity-enhanced dual-optical comb spectroscopy that enables CE-DCS with mode-resolved resolution, broad bandwidth, and high sensitivity. The adaptive corrections of the IGMs achieve a resolution of 250 MHz with a compact and simplified setup. The adaptive comb-cavity coupling allows tighter locking, wider bandwidth, and an increase in the number of the total spectral elements. Unlike the two-point locking scheme [7,8], our scheme locks the cavity to the comb. Thus, no strict vibration and thermal control are required for the cavity, and the comb could be locked to highly stable frequency standards, such as atomic clocks, which in turn permits excellent stability and traceability. Compared with the previous adaptive DCSs [30,32], the measurement sensitivity is improved more than 2 orders of magnitude because of the enhanced cavity. Given that no additional CW lasers are needed, since the lasers used for measuring the dual-comb jitters can also be used for coupling the cavity, very little increase in complexity is introduced. Considering the advantages of the DCS, which are the elimination of moving parts and the high measurement speed, this ACE-DCS technique is expected to benefit many precise spectrometry applications. It is especially true for the investigation of atmospheric observation and combustion diagnosis, where it requires not only high resolution and sensitivity but also the need for dynamic and multiplex analysis. By adopting cavity mirrors with higher reflectivity, this ACE-DCS system can enable broadband spectral measurements for the applications that require extremely high sensitivity, such as trace-gas detection and radiocarbon chronology. These advantages could mean they will surpass and replace CW laser-based spectral measuring techniques and show huge potential to promote fundamental science.

APPENDIX A: POSTCORRECTION ALGORITHM

The details of the postcorrection algorithm are illustrated in Fig. 5 and have two major steps: mixing and resampling [39].

First, the mixing step is used to neutralize the mutual jitter of the difference of f_{ceo}, represented by Δf_{ceo}. Specifically, the two CW lasers produce beat notes at the frequencies around their adjacent comb modes: the numbers of p_1 and p_2 modes of Comb1 and those of q_1 and q_2 of Comb2, respectively. In our configuration, we chose a difference of repetition rate (df_{ceo}) to the one that makes the value of q_1 equal to p_1 and q_2 equal to p_2, helping avoid frequency aliasing. Besides, we actually recorded only three beat notes (Beats 2, 3, and 4 in Fig. 5) and digitally constructed the last one (Beat 1 in Fig. 5). The recording of these beat notes was synchronized with that of the dual-comb IGMs. In terms of processing, we extracted the phase of the beat notes derived between the two combs and the same CW laser (φ_{11} and φ_{12} for CW1, φ_{21} and φ_{22} for CW2) and calculated the difference between the two (φ_1 and φ_2). These two phases represent the phase change between the two combs at the frequencies of the CW1 and CW2 lasers and can be expressed as Eqs. (A1) and (A2). Then, as shown in Fig. 5, we produced a φ_0 using the value of φ_1 and add ($n \times \Delta\varphi$), where n is an integer. This step is to get a φ_0 so that the frequency of the $\cos(\varphi_0)$ lies outside the frequency of the IGMs. Subsequently, we mixed the IGMs with the $\cos(\varphi_0)$ and applied low-pass filtering to the product. Because the φ_0 contains the jitter of f_{ceo}, the Δf_{ceo} shown in Eq. (A4), the mixed IGMs are free from the influence of f_{ceo} and only consist of multiples of the repetition rate difference and its jitter (df_{rep} and Δf_{rep}):

$$\varphi_1 = q_1 \times (f_{rep2} - f_{rep1}) + (f_{ceo2} - f_{ceo1}), \quad \textbf{(A1)}$$

$$\varphi_2 = q_2 \times (f_{rep2} - f_{rep1}) + (f_{ceo2} - f_{ceo1}), \quad \textbf{(A2)}$$

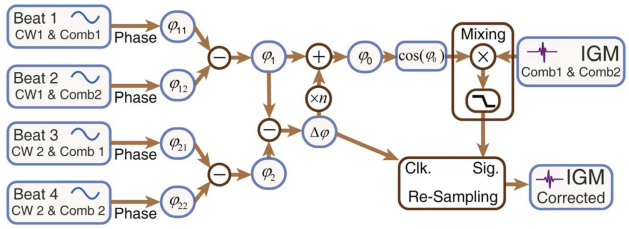

Fig. 5. Diagram for the postcorrection algorithm. Clk., clock; Sig., signal.

$$\Delta\varphi = (q_2 - q_1) \times (f_{rep2} - f_{rep1}) = (q_2 - q_1) \times (\mathrm{d}f_{rep} + \Delta f_{rep}), \quad \textbf{(A3)}$$

$$\varphi_0 = (q_1 + n) \times (\mathrm{d}f_{rep} + \Delta f_{rep}) + \mathrm{d}f_{ceo2} + \Delta f_{ceo}. \quad \textbf{(A4)}$$

Second, the resampling could eliminate the jitter of the repetition rate on the IGMs. Specifically, we took the $\Delta\varphi$, shown in Eq. (A3), as a reference coordinate and resampled the IGMs by interpolation and at a specified interval on this coordinate. To avoid the loss of accuracy and the increase of the data size, the resampling interval was assigned to one that maintained the lengths of the resampled IGMs close to the original ones. After that, the resampled IGMs were free from the effects of both the f_{rep} jitters and the f_{ceo} jitters.

Funding. National Natural Science Foundation of China (NSFC) (61775114).

REFERENCES

1. B. Spaun, P. B. Changala, D. Patterson, B. J. Bjork, O. H. Heckl, J. M. Doyle, and J. Ye, "Continuous probing of cold complex molecules with infrared frequency comb spectroscopy," Nature **533**, 517–520 (2016).
2. B. J. Bjork, T. Q. Bui, O. H. Heckl, P. B. Changala, B. Spaun, P. Heu, D. Follman, C. Deutsch, G. D. Cole, M. Aspelmeyer, M. Okumura, and J. Ye, "Direct frequency comb measurement of OD + CO → DOCO kinetics," Science **354**, 444–448 (2016).
3. C. A. Alrahman, A. Khodabakhsh, F. M. Schmidt, Z. Qu, and A. Foltynowicz, "Cavity-enhanced optical frequency comb spectroscopy of high-temperature H_2O in a flame," Opt. Express **22**, 13889–13895 (2014).
4. M. J. Thorpe, D. Balslev-Clausen, M. S. Kirchner, and J. Ye, "Cavity-enhanced optical frequency comb spectroscopy: application to human breath analysis," Opt. Express **16**, 2387–2397 (2008).
5. S. Coburn, C. B. Alden, R. Wright, K. Cossel, E. Baumann, G.-W. Truong, F. Giorgetta, C. Sweeney, N. R. Newbury, K. Prasad, I. Coddington, and G. B. Rieker, "Regional trace-gas source attribution using a field-deployed dual frequency comb spectrometer," Optica **5**, 320–327 (2018).
6. K. C. Cossel, E. M. Waxman, F. R. Giorgetta, M. Cermak, I. R. Coddington, D. Hesselius, S. Ruben, W. C. Swann, G.-W. Truong, G. B. Rieker, and N. R. Newbury, "Open-path dual-comb spectroscopy to an airborne retroreflector," Optica **4**, 724–728 (2017).
7. R. J. Jones, I. Thomann, and J. Ye, "Precision stabilization of femtosecond lasers to high-finesse optical cavities," Phys. Rev. A **69**, 051803 (2004).
8. R. J. Jones and J.-C. Diels, "Stabilization of femtosecond lasers for optical frequency metrology and direct optical to radio frequency synthesis," Phys. Rev. Lett. **86**, 3288–3291 (2001).
9. A. Foltynowicz, T. Ban, P. Masłowski, F. Adler, and J. Ye, "Quantum-noise-limited optical frequency comb spectroscopy," Phys. Rev. Lett. **107**, 233002 (2011).
10. N. Hoghooghi, R. J. Wright, A. S. Makowiecki, W. C. Swann, E. M. Waxman, I. Coddington, and G. B. Rieker, "Broadband coherent cavity-enhanced dual-comb spectroscopy," Optica **6**, 28–33 (2019).
11. F. Adler, M. J. Thorpe, K. C. Cossel, and J. Ye, "Cavity-enhanced direct frequency comb spectroscopy: technology and applications," Annu. Rev. Anal. Chem. **3**, 175–205 (2010).
12. M. J. Thorpe and J. Ye, "Cavity-enhanced direct frequency comb spectroscopy," Appl. Phys. B **91**, 397–414 (2008).
13. M. J. Thorpe, K. D. Moll, R. J. Jones, B. Safdi, and J. Ye, "Broadband cavity ringdown spectroscopy for sensitive and rapid molecular detection," Science **311**, 1595–1599 (2006).
14. L. C. Sinclair, K. C. Cossel, T. Coffey, J. Ye, and E. A. Cornell, "Frequency comb velocity-modulation spectroscopy," Phys. Rev. Lett. **107**, 093002 (2011).
15. M. J. Thorpe, F. Adler, K. C. Cossel, M. H. G. de Miranda, and J. Ye, "Tomography of a supersonically cooled molecular jet using cavity-enhanced direct frequency comb spectroscopy," Chem. Phys. Lett. **468**, 1–8 (2009).
16. S. A. Diddams, L. Hollberg, and V. Mbele, "Molecular fingerprinting with the resolved modes of a femtosecond laser frequency comb," Nature **445**, 627–630 (2007).
17. L. Rutkowski and J. Morville, "Continuous Vernier filtering of an optical frequency comb for broadband cavity-enhanced molecular spectroscopy," J. Quantum Spectrosc. Radiat. Transfer **187**, 204–214 (2017).
18. L. Rutkowski and J. Morville, "Broadband cavity-enhanced molecular spectra from Vernier filtering of a complete frequency comb," Opt. Lett. **39**, 6664–6667 (2014).
19. C. Gohle, B. Stein, A. Schliesser, T. Udem, and T. W. Hänsch, "Frequency comb Vernier spectroscopy for broadband, high-resolution, high-sensitivity absorption and dispersion spectra," Phys. Rev. Lett. **99**, 263902 (2007).
20. L. Rutkowski, A. C. Johansson, G. Zhao, T. Hausmaninger, A. Khodabakhsh, O. Axner, and A. Foltynowicz, "Sensitive and broadband measurement of dispersion in a cavity using a Fourier transform spectrometer with kHz resolution," Opt. Express **25**, 21711–21718 (2017).
21. A. J. Fleisher, D. A. Long, Z. D. Reed, J. T. Hodges, and D. F. Plusquellic, "Coherent cavity-enhanced dual-comb spectroscopy," Opt. Express **24**, 10424–10434 (2016).
22. B. Bernhardt, A. Ozawa, P. Jacquet, M. Jacquey, Y. Kobayashi, T. Udem, R. Holzwarth, G. Guelachvili, T. W. Hänsch, and N. Picqué, "Cavity-enhanced dual-comb spectroscopy," Nat. Photonics **4**, 55–57 (2010).
23. M. L. Weichman, P. B. Changala, J. Ye, Z. Chen, M. Yan, and N. Picqué, "Broadband molecular spectroscopy with optical frequency combs," J. Mol. Spectrosc. **355**, 66–78 (2019).
24. N. Picqué and T. W. Hänsch, "Frequency comb spectroscopy," Nat. Photonics **13**, 146–157 (2019).
25. Z. Chen, M. Yan, T. W. Hänsch, and N. Picqué, "A phase-stable dual-comb interferometer," Nat. Commun. **9**, 3035 (2018).
26. I. Coddington, N. Newbury, and W. Swann, "Dual-comb spectroscopy," Optica **3**, 414–426 (2016).
27. I. Coddington, W. C. Swann, and N. R. Newbury, "Coherent multiheterodyne spectroscopy using stabilized optical frequency combs," Phys. Rev. Lett. **100**, 013902 (2008).
28. P. Giaccari, J.-D. Deschênes, P. Saucier, J. Genest, and P. Tremblay, "Active Fourier-transform spectroscopy combining the direct RF beating of two fiber-based mode-locked lasers with a novel referencing method," Opt. Express **16**, 4347–4365 (2008).
29. X. Shen, M. Yan, Q. Hao, K. Yang, and H. Zeng, "Adaptive dual-comb spectroscopy with 1200-h continuous operation stability," IEEE Photon. J. **10**, 1503309 (2018).
30. T. Ideguchi, A. Poisson, G. Guelachvili, N. Picqué, and T. W. Hänsch, "Adaptive real-time dual-comb spectroscopy," Nat. Commun. **5**, 3375 (2014).
31. Z. Zhu, K. Ni, Q. Zhou, and G. Wu, "Digital correction method for realizing a phase-stable dual-comb interferometer," Opt. Express **26**, 16813–16823 (2018).
32. J. Roy, J.-D. Deschênes, S. Potvin, and J. Genest, "Continuous real-time correction and averaging for frequency comb interferometry," Opt. Express **20**, 21932–21939 (2012).
33. J.-D. Deschênes, P. Giaccari, and J. Genest, "Optical referencing technique with CW lasers as intermediate oscillators for continuous full delay range frequency comb interferometry," Opt. Express **18**, 23358–23370 (2010).
34. G. W. Truong, K. O. Douglass, S. E. Maxwell, R. D. van Zee, D. F. Plusquellic, J. T. Hodges, and D. A. Long, "Frequency-agile, rapid scanning spectroscopy," Nat. Photonics **7**, 532–534 (2013).
35. A. J. Fleisher, D. A. Long, and J. T. Hodges, "Quantitative modeling of complex molecular response in coherent cavity-enhanced dual-comb spectroscopy," J. Mol. Spectrosc. **352**, 26–35 (2018).
36. I. E. Gordon, L. S. Rothman, C. Hill, R. V. Kochanov, Y. Tan, P. F. Bernath, M. Birk, V. Boudon, A. Campargue, K. V. Chance, B. J. Drouin, J. M. Flaud, R. R. Gamache, J. T. Hodges, D. Jacquemart, V. I. Perevalov, A. Perrin, K. P. Shine, M. A. H. Smith,

J. Tennyson, G. C. Toon, H. Tran, V. G. Tyuterev, A. Barbe, A. G. Császár, V. M. Devi, T. Furtenbacher, J. J. Harrison, J. M. Hartmann, A. Jolly, T. J. Johnson, T. Karman, I. Kleiner, A. A. Kyuberis, J. Loos, O. M. Lyulin, S. T. Massie, S. N. Mikhailenko, N. Moazzen-Ahmadi, H. S. P. Müller, O. V. Naumenko, A. V. Nikitin, O. L. Polyansky, M. Rey, M. Rotger, S. W. Sharpe, K. Sung, E. Starikova, S. A. Tashkun, J. V. Auwera, G. Wagner, J. Wilzewski, P. Wcisło, S. Yu, and E. J. Zak, "The HITRAN2016 molecular spectroscopic database," J. Quantum Spectrosc. Radiat. Transfer **203**, 3–69 (2017).

37. A. Foltynowicz, P. Masłowski, T. Ban, F. Adler, K. C. Cossel, T. C. Briles, and J. Ye, "Optical frequency comb spectroscopy," Faraday Discuss. **150**, 23–31 (2011).
38. W. Zhang, H. Wei, X. Chen, and Y. Li, "Sensitivity improvement by optimized optical switching and curve fitting in a cavity ring-down spectrometer," Appl. Opt. **57**, 8487–8493 (2018).
39. X. Chen, W. Zhang, H. Wei, and Y. Li, "Digitally calibrated broadband gases absorption spectral measurements," Chin. Phys. B **28**, 060703 (2019).